Covariability of Climate and Upper Rio Grande Streamflow

Madeleine Pascolini-Campbell,[1] Richard Seager,[2] Ariane Pinson,[3] and

Benjamin I. Cook[4]

Corresponding author Tel: +1 347346009 email: map2251@columbia.edu

[1]Department of Earth and Environmental Sciences, Columbia University, New York, USA.

[2]Lamont Doherty Earth Observatory of Columbia University, Palisades, New York, USA.

[3]United States Army Corps of Engineers, Albuquerque District, Albuquerque, New Mexico, USA

[4]NASA Goddard Institute for Space Studies, New York, USA

Key Points.

(streamflow; decadal; Rio Grande; ENSO; AMO; PDO)

Abstract. Upper Rio Grande streamflow variability is explained on timescales of months to decades by the combined influence of the El Niño-Southern Oscillation (ENSO), Pacific Decadal Oscillation (PDO), Atlantic Multidecadal Oscillation (AMO) and the North American Monsoon (NAM). The peak in spring-summer streamflow has a positive relationship with Pacific sea surface temperature (SST), and a negative relationship with north Atlantic SST. On monthly timescales, the relationship between streamflow and Pacific SST is nonlinear: warm Pacific episodes produce above normal streamflow, but cold Pacific episodes have a more varied response in streamflow. On annual timescales, El Niño episodes generally increase the magnitude of upper Rio Grande streamflow. The upper Rio Grande is also characterized by decadal variability: periods of high flow and precipitation (1900-1920 and 1979-1994) are found to coincide with the positive PDO and negative AMO phases. Cyclonic flow off the United States west coast, and anomalous moisture convergence located over the upper Rio Grande region, is also prevalent during winters in these high flow decades. The strength of these teleconnections increases toward the south of the basin, where Pacific SST forcing is more important. SST teleconnections and its influence on basin precipitation is found to be more important in the winter preceding spring-summer streamflow. These configurations of ocean and atmosphere explain the observed variability of

upper Rio Grande streamflow and provide predictability, which is essential for its effective management and the millions of people relying on its waters.

1. Introduction

The Rio Grande flows from the San Juan Mountains of Colorado south through the United States in New Mexico followed by Texas where it serves as the border between the United States and Mexico. With a length of 3,051 km and a drainage area of approximately 472,000 km^2, it is one of the longest rivers in the United States. It is heavily managed, providing water to 5 million people for a variety of purposes including domestic use, industry and irrigation [*Woodhouse et al.*, 2012]. The upper Rio Grande is particularly important because it provides much of the water to the lower Rio Grande system as well as the Elephant Butte Reservoir, an essential water source for irrigation in New Mexico.

The headwaters streamflow is controlled by the magnitude and timing of the melting of the winter snowpack. Further south, the river also receives inputs from its main tributary, the Rio Conchos, which is influenced by the summer North American Monsoon [*Woodhouse et al.*, 2013]. The Rio Grande has experienced drought for over the past decade [*Woodhouse et al.*, 2013], with below average flows since 2000. In addition the flow is highly variable year to year, posing challenges to management. Improved understanding of the climate controls on Rio Grande flow variability is essential to improve management of water resources.

Previous work has shown that streamflow in the United States southwest in general is affected by a range of drivers including the El Niño-Southern Oscillation (ENSO), the Pacific Decadal Oscillation (PDO), the Atlantic Multidecadal Oscillation (AMO) and the North American Monsoon (NAM). All factors impact runoff to the rivers via the regional

interaction of precipitation, evapotranspiration, snowmelt, soil moisture and vegetation [*Notaro et al.*, 2010]. Studies indicate that ENSO produces above normal precipitation and streamflow for the southwest when it is in its warm phase (El Niño) [*Kahya and Dracup*, 1993,]. The PDO has also been found to produce above normal precipitation and streamflow during its positive phase [*Barlow et al.*, 2001; *Cayan et al.*, 1999; *Pascolini-Campbell et al.*, 2015]. The AMO has an inverse relationship with southwest streamflow and precipitation [*Enfield et al.*, 2001; *Thomas*, 2007; *Nowak et al.*, 2012].This relationship is strengthened with a concurrent positive PDO phase [*McCabe et al.*, 2004]. The NAM brings a summer (July-August-September (JAS)) peak in rainfall [*Adams and Comrie*, 1997; *Barlow et al.*, 1998] and NAM variability presumably drives streamflow variability [*Pascolini-Campbell et al.*, 2015].

Studies have also examined the individual impacts of the ENSO, PDO, AMO and NAM on upper Rio Grande streamflow. Generally the results are consistent with the studies of regional southwest flow variability. Several authors have noted the importance of winter snowfall and its subsequent melt, in generating spring runoff into the river [*Lee et al.*, 2004; *Khedun et al.*, 2010; *Woodhouse et al.*, 2012]. The positive impact of ENSO in producing above-normal precipitation and streamflow anomalies in the upper Rio Grande basin during El Niño episodes has also been confirmed [*Lee et al.*, 2004; *Khedun et al.*, 2010]. Looking at precipitation, snow water equivalent, temperature, streamflow and the Southern Oscillation Index (SOI), one study found that the ENSO influence is seasonally dependent: a stronger impact on temperature, rainfall and snowfall occurs at the beginning (November) and end (March) of the winter [*Lee et al.*, 2004]. An investigation using the Noah land surface model to generate runoff, found the influence of El Niño events

varies: longer duration events produce stronger positive Rio Grande flow anomalies than shorter, more intense events [*Khedun et al.*, 2010]. PDO has also been found to produce above normal precipitation and streamflow in the upper Rio Grande during its positive phase, particularly when coupled with an El Niño episode [*Khedun et al.*, 2010]. These studies have helped elucidate the different roles played by ENSO, PDO, AMO and NAM on producing upper Rio Grande streamflow variability.

Characterizing the streamflow and precipitation response within the upper Rio Grande to ENSO, PDO, AMO and NAM is particularly important in light of recent studies suggesting these systems may change or strengthen with a warming climate (e.g. [*Ting et al.*, 2014; *Cai et al.*, 2015; *Ruff et al.*, 2011]). Changes in ENSO and its teleconnections, in particular, could have potentially serious implications for the arrival of winter storms which deposit precipitation in the Southwest United States [*Larkin and Harrison*, 2005]. Studies using modeling have also indicated that greenhouse gas (GHG) warming could delay both NAM onset and retreat [*Seth et al.*, 2013; *Cook and Seager*, 2013]. Further, the upper Rio Grande region has warmed by 1.5°C since 1970 [*Llewellyn and Vaddey*, 2013]. This has led to a shift to earlier snowpack melt and peak streamflow in the southwest [*Stewart et al.*, 2005; *Fritze et al.*, 2011], and also could increase evapotranspiration at the expense of runoff and streamflow [*Hurd and Coonrod*, 2008; *Gutzler*, 2013].

Despite these advances no current research explicitly examines the combined role of ENSO, PDO, AMO and the NAM on the upper Rio Grande. But an understanding of teleconnections between climate and flow is necessary for effective water management in the current and future climate. While work on the connection of Pacific and Atlantic variability with Southwest United States hydrology [*Kahya and Dracup*, 1993, ; *Barlow*

et al., 2001; *Cayan et al.*, 1999; *McCabe et al.*, 2004], and on the Rio Grande response to ENSO [*Lee et al.*, 2004; *Khedun et al.*, 2010] exist, these studies only examine the individual impacts of the different teleconnections rather than the combined effect. The aggregate influence of these drivers still remains to be investigated.

The present study aims to fill this gap by using upper Rio Grande stream gage data, observed precipitation, observed ocean SST and atmospheric reanalysis output to provide a more complete understanding of upper Rio Grande streamflow variability and the combined role of ENSO, PDO, AMO, NAM and associated atmospheric circulation, over the past several decades. Configurations of SST and atmospheric conditions conducive to high anomalies are also examined. The following questions are investigated:

- What configuration of ocean SST (including both Pacific and Atlantic oceans) and atmospheric circulation anomalies drive flow variability for the upper Rio Grande?
- In which seasons are these climate teleconnections most significant?
- Which atmosphere-ocean configurations produce extreme monthly flow events?
- Does the decadal scale flow variability correspond to distinct atmosphere-ocean states?
- How does the precipitation and streamflow response to these drivers vary geographically within the upper Rio Grande basin?

This investigation will advance understanding of the climate controls on upper Rio Grande flow variability and extreme high flows to the benefit of water management activities.

2. Data and Methods

To analyze the natural drivers of Rio Grande streamflow at its headwaters, seven United States Geological Survey Gages (USGS) of tributaries in New Mexico are selected and compared with two gages located on the Rio Grande main stem (see Figure 1 for location). Tributaries are selected because all stream gages on the Rio Grande main stem are affected by human activity and water withdrawals. Instead the following unmodified New Mexico tributaries are selected (arranged from northernmost to southernmost): Rio Chama near La Puente (USGS 08284100), Santistevan Creek near Costilla (USGS 08253500), Rio Hondo near Valdez (USGS 08267500), Rio Lucero near Arroyo Seco (USGS 08271000), Rio Pueblo de Taos near Taos (USGS 08269000), Rio Ojo Caliente near Madera (USGS 08289000) and Jemez River near Jemez (USGS 08324000). The stream flows of these rivers are compared to two upstream gages lying on the main Rio Grande stem itself (Rio Grande near Del Norte, CO, (USGS 08220000), and Rio Grande at Otowi Bridge, New Mexico, (USGS 08313000)) (time period available shown in Table 1). Pearson's correlation is used throughout to assess the strength of the relationships between variables. High correlation ($r = 0.75$ to $r = 0.87$) is found to exist between the Rio Grande gages and the tributary flows, thus allowing the tributaries to serve as suitable indicators of the natural flow variability (Table 1, last column). These gages are located in the upper reaches of the Rio Grande in an area characterized by mountainous terrain with peaks exceeding 3500 m. The area receives precipitation as snow during winter months, which melts in the spring and summer. Rainfall is greatest in the summer months when the area is affected by local-scale convective activity. Monthly and daily streamflow data are used for these sites to examine flow.

The precipitation dataset used is from the Parameter Regression on Independent Slopes Model (PRISM; in units of mm/month on a 4km grid), which uses a well-verified, terrain-sensitive algorithm to interpolate between available stations over the period 1895-present [*Daly et al.*, 2008]. Precipitation is averaged over the catchment area of each of the stream gages to investigate local variability. For SST, ERSST V3 reanalysis data (in units of degrees Celsius on a 2°x2° global grid) are used [*Smith et al.*, 2008]. Monthly sea level pressure (SLP) data from NCEP-NCAR Reanalysis (on a 2.5°x2.5° global grid) is used [*Kalnay et al.*, 1996]. ERA Interim data for vertically integrated moisture flux are used to analyze the atmospheric moisture delivery patterns (1.5°x1.5° global grid) (1979 - 2014) [*Dee et al.*, 2011].

First, analysis will cover the period of the full flow records (see Table 1) to investigate flow timeseries, hydrographs, associated precipitation and temperature trends for each catchment area and their correlation with flow. Following this, the focus will be on 1979 - 2014 to match the temporal availability of the ERA Interim dataset.

3. Results

3.1. Climatology and variability of upper Rio grande streamflow, precipitation and temperature

The water year mean streamflow for the tributaries Rio Chama, Santistaven, Hondo, Lucero, Pueblo, Ojo and Jemez stream gages are found to be highly correlated with those of Del Norte and Otowi on the main stem of the Rio Grande (Table 1, last column). The timing of the peak flow is also found to be fairly consistent between the main stem and the tributaries with highest flows occurring in April-May-June-July (Figure 2). Gages further north in the basin (Del Norte, Rio Chama, Santistaven, Hondo and

Lucero) are found to have peak flows occurring more in May-June, whereas gages more south in the basin (Pueblo, Ojo, Otowi and Jemez) have peak flows occuring earlier in April-May-June. This is consistent with earlier snowmelt occurring further south in the basin contributing to earlier spring-summer flows (see Figure 4 below). The similar timing in streamflow is expected given the proximity of these stream gages, as well as their comparable elevations in the basin (Table 1). The hydrographs (Figure 2) also illustrate the positive skew of the data: many of the highest flows exceed 1.5 times the interquartile range of the data (as demonstrated by the outliers denoted by a red cross). Figure 4 (top panel) shows the timeseries of mean water year flow. Similar timing in anomalously high flows is observed to occur between the different gages, such as the high flow peaks in 1985, 1995 and 2005. Magnitudes are far smaller for the tributaries which drain much smaller basins in the system such as Hondo, Lucero and Pueblo (see Table 1 for drainage area). The water year timeseries in Figure 4 also contain a similar decadal pattern of high flow centered around 1985 and declining flow from 1990 to present. In the longer streamflow timeseries (for Del Norte) this decadal variability is seen to also produce above normal flow in the early century (1900-1920) and lower flow in 1945 to 1975.

The seasonal cycles of precipitation and temperature are investigated using PRISM data averaged over the area of the stream gage (Figure 3). Precipitation over the more northern gages (Del Norte, Rio Chama, Santistaven, Rio Hondo and Rio Lucero) displays a bimodal peak: the first occurring in February-March-April (reaching a maximum of 75 mm/month for Rio Chama), and the second in July-August-September (reaching a maximum of approximately 75 mm/month for Rio Chama, Santistaven and Lucero). The more southern gages (Pueblo, Ojo, Otowi and Jemez) have a more pronounced summer

precipitation maximum (June-July-August) indicative of the monsoon influence. For the more northern gages, the minimum monthly temperature is below freezing from October to June, and the maximum monthly temperature falls below freezing in November-December-January. It can be inferred that snowmelt could occur anytime after January but snow could last through spring. The more southern gages also drain areas starting at a lower elevation (see Table 1), and have minimum temperatures that are below zero from October to May, and maximum temperatures that never fall below freezing. Snowmelt here, derived from lower elevation drainage areas than the northern counterparts, can be expected to begin earlier in the year as temperatures rise above freezing.

The longterm timeseries of PRISM precipitation area-averaged for each tributary station are illustrated in Figure 4 from 1895 to 2014. The majority of gages indicate a period of wetter than average conditions in the early 20th century (1900 - 1920) followed by a decline in the mid-century to drier than average conditions (from approximately 1945 to 1975). The precipitation decadal mean then increases again from the 1980s to around 2000 after which it again tends to decline. This variability is consistent with the decadal water year streamflow in Figure 4 (top panels).

3.2. Relation of peak flow variability to antecedent precipitation and atmosphere-ocean states

The peak streamflow is averaged over April-May-June-July (AMJJ) and the log-value of this timeseries is correlated with the current October to July monthly PRISM precipitation averaged over each tributary drainage basin (Figure 5). Results indicate that AMJJ streamflow is most correlated with winter and spring (October to May) pre-

cipitation, with correlation for all months being about equal (range of r = 0.5 to r = 0.6).

Nationwide correlations between AMJJ streamflow at upper Rio Grande Gages and precipitation reveal strong positive and negative relationships.The precipitation over the entire United States during winter (December-January-February (DJF)) and spring (March-April-May (MAM)) is then correlated with AMJJ streamflow (Figure 6). During winter, greatest correlation occurs in the United States southwest with r-values exceeding r = 0.5. There is a negative correlation in the Pacific Northwest region of the United States. The region of positive correlation is more widespread for the southern gages during DJF. During spring, the positive anomaly is centered directly over the region of the gages with correlations reaching r = 0.75. Negative correlations exist over the northeast United States at this time.

Because the spatial correlations between AMJJ stream flow and precipitation nationwide are similar to that proposed for El Niño-induced precipitation teleconnection [*Ropelewski and Halpert*, 1986, ,], the relationship between AMJJ streamflow and SSTs in the Pacific and Atlantic were then investigated (Figure 7). AMJJ streamflow is positively correlated (r=0.5) with eastern and equatorial Pacific SSTs, and negatively correlated with western Pacific and Atlantic SSTs. These relationships are consistent with previous studies that identify the role of ocean-driven teleconnections on North American precipitation and streamflow [*Cayan et al.*, 1999; *Enfield et al.*, 2001; *Thomas*, 2007; *Nowak et al.*, 2012], and indicate that ENSO may play a strong role in determining patterns of stream flow in the study area. The strength of the Pacific correlation is greatest for the most southern gage (Jemez) and weakest at the most northern gage (Del Norte). The correlation results for

MAM SST have a similar pattern of correlation in the Pacific, although this relationship is weaker than for DJF SSTs.

For each water year, the maximum monthly flow is found and plotted along with the value of the NINO3.4 DJF index (Figure 8, separately for the three most northern gages (Del Norte, Rio Chama, Santistaven), the middle gages (Hondo, Lucero and Pueblo) and the most southern gages (Ojo, Otowi and Jemez)). Results indicate that high flows typically correspond with positive NINO3.4 DJF values. The most northern gages correspond less strongly with NINO3.4 SST (maximum r = 0.25) than the middle and southern gages (maximum r = 0.31) (Figure 8). This is consistent with the ENSO precipitation teleconnection pattern being stronger in the southern half of the upper Rio Grande region. Low flows are more weakly correlated with the sign of the DJF NINO3.4 index, suggesting a weaker causal role for SST teleconnections in low flow conditions than high flow conditions. .

To examine the impact of individual El Niños in producing high streamflow, USGS daily streamflow data are used to create hydrographs showing the spread of flow anomalies occurring during the 1982/83, 1986/87, 1991/92, 1997/98, 2002/03, 2004/05, 2006/07 and 2009/10 episodes (Figure 9). The longterm daily mean data for each gage are also plotted. Hydrographs during El Niño events in general are found to have higher magnitude flow anomalies than the long term daily mean, consistent with Figure 8. Gages further south in the basin where flows were more highly correlated with ENSO (as shown in Figure 7) also tend to display higher magnitude flow anomalies associated with El Niño events. For example, Jemez experienced more than four times its mean flow. Flow increases above the daily mean at Del Norte during El Niño events show more modest increases on the order

of two times the daily mean. The spread of flow anomalies compared to the longterm daily mean suggests that although there is generally larger magnitude flow, there is no general relationship between peak flow timing and El Niño events, with some peaking earlier and others lasting longer. The exception is for Santistaven, in which the El Niño mean lags the longterm daily mean streamflow.

Following from the finding of a positive (negative) relationship with the Pacific (Atlantic) to streamflow, a linear multiple regression using DJF NINO3.4 and Tropical North Atlantic (TNA) (SST averaged over the Atlantic from 0° to 30°N) as predictors is used to model AMJJ streamflow (Figure 10). Results from an Akaike Information Criterion test (not shown) indicate the multiple regression model performs better in modeling streamflow than using either index on its own. The R^2 values indicate that total variance explained is lower for northern gages (R^2=0.07 for Del Norte) and higher for the southern gages (R^2 =0.18 at Jemez), indicating a greater control of SST on streamflow variability in the southern regions. Including both ocean basins increases the total variance explained, however, it is also noted that a large part of the variance in AMJJ streamflow is not explained by either Pacific nor north Atlantic SST variability.

3.3. Atmosphere-ocean states corresponding to top 10 monthly flows

Next the top 10 monthly flows from 1979 to 2014 are identified. The top 10 monthly flows for each gage occur exclusively during the spring-summer months of April-May-June-July. and are plotted for the months in which they occur, along with concurrent and preceding flow and precipitation anomalies for Del Norte, Pueblo and Jemez (Figure 11). These three gages are selected to represent different positions spanning north to south within the upper Rio Grande region. For the more northern gages with summer

flow maxima, and the more southern gages with spring flow maxima, a wide variety of precipitation anomalies can be responsible. In general, however, high winter precipitation preceded the high flows in all gages and in only one case (a June high flow at Del Norte) does high spring precipitation appear causal.

Next, the atmosphere configuration corresponding to the top 10 monthly flows are identified. Composites for the top 10 monthly flows for these same three gages, are created for the preceding winter (DJF) and spring (MAM) for ERA Interim vertically integrated moisture transport anomaly and its divergence (Figure 12). Anomalous DJF moisture convergence (blue shading) over the southwest region is clear for Pueblo and Jemez but also true for Del Norte. Cyclonic flow (vectors) occurs west of the southwest region during DJF preceding high flows such that the Rio Grande is under moistening southerly flow, again most clear for Pueblo and Jemez. The MAM moisture transport in the southwest is either weakly convergent or even divergent, consistent with the SST correlations in Figure 7 which show a general dominance of winter precipitation anomalies on the maximum late spring-early summer flow anomalies.

Composites for the top 10 monthly flows are also created for DJF and MAM SST (Figure 13). Consistent with Figures 7 and 8, the composites illustrate a stronger El Niño pattern occurring for gages further south in the basin and for winter than spring. The DJF composites also indicate a cold North Atlantic suggesting the expected negative relationship between high streamflow and the AMO.

Composites of precipitation for the top 10 monthly flows for DJF and MAM indicate positive anomalies over the gages in winter (Figure 14, top panels), with weaker but broader positive anomalies over the south western United States in spring (Figure

14, bottom panels). These positive anomalies are consistent with ENSO precipitation teleconnections for the US southwest [*Ropelewski and Halpert*, 1986, ,], and therefore consistent with the El Niño SST patterns shown in Figure 7 and 13. They also are consistent with the anomalous moisture convergence observed in DJF (Figure 12).

3.4. Climatic causes of decadal variability of upper Rio Grande flow

Decadal flow patterns are examined by focusing on the notable changes in flow of Del Norte and Otowi between the early and mid parts of the last century (Figure 4). Figure 15 contains composites for the dry (1945-1975) minus the detrended 20th century climatology and wet (1900-1920) decades minus the detrended 20th century climatology in both water year PRISM precipitation and DJF ERSST V4 SST. For the dry composite, widespread negative precipitation occurs over the southwestern United States including the region of the Upper Rio Grande. The early composite indicates wet anomalies over the southwest in a region more centered over the Rio Grande basin. The early wet period is the early 20th century North American pluvial of 1900 to 1917 [*Cook et al.*, 2011]. The pattern of DJF SST for the dry years indicate a region of cooling in the equatorial Pacific and along the North American west coast, positive anomalies in the North Pacific and positive anomalies in the North Atlantic (Figure 15, bottom left panel). This decadal pattern of SST is consistent with the cool phase of the PDO (characterized by a cool equatorial Pacific and warm North Pacific [*Zhang et al.*, 1997]), and the warm phase of the AMO [*Enfield et al.*, 2001], ideal conditions for a wetter than normal climate in the southwest [*Schubert*, 2009]. The composite for wet years indicates a warm equatorial Pacific, cool north Pacific and warm Atlantic. This configuration represents a warm PDO and cold AMO phase.

Figure 16 examines decadal variability from 1979 to present for the two halves of the water year (October to March and April to September) in SST, SLP and moisture transport. For October to March, the dry decades (1994 -2014) minus the wet decades (1979-2014) shows negative SST anomalies in the equatorial Pacific and positive anomaly in the North Pacific, positive SLP anomalies in the Pacific and anticyclonic circulation (vectors) with moisture divergence over the Rio Grande. This pattern is consistent with the negative phase of the PDO which has been associated with below normal streamflow and precipitation in the southwest [*Zhang et al.*, 1997; *Barlow et al.*, 2001; *Cayan et al.*, 1999; *Pascolini-Campbell et al.*, 2015]. The magnitude of the anomalies are reduced in April to September.

Annually-averaged water year flow is also compared between Del Norte on the Rio Grande and naturalized Lee's Ferry streamflow on the Colorado River and the two series are found to be highly correlated (r = 0.80). This suggests that, despite differences in the location of the drainage basins, similar drivers may be responsible for determining the flow and character of each river.

4. Discussion and Conclusions

This study has examined how ocean-atmosphere configurations influence upper Rio Grande streamflow variability. We extend previous research on the influence of ENSO and PDO on streamflow [*Lee et al.*, 2004; *Khedun et al.*, 2010], to pinpoint the roles of the Pacific and Atlantic oceans as well as atmospheric anomalies in modulating streamflow. Ocean-atmosphere configurations are used to explain upper Rio Grande streamflow variability on a variety of scales: monthly, seasonal and decadal. The conditions conducive to producing extreme monthly streamflows are also investigated.

1. On monthly time-scales, the ocean configuration favoring above normal upper Rio Grande streamflow consists of a warm equatorial Pacific and cold north Atlantic. This SST configuration is consistent with the well documented influence of a warm tropical Pacific producing a north-east propagating Rossby wave train and positive precipitation anomalies in the U.S. southwest [*Trenberth et al.*, 1998]. A cold North Atlantic is also known to enhance the impact of the ENSO warm phase teleconnection resulting in positive precipitation anomalies [*Enfield et al.*, 2001; *McCabe et al.*, 2004]. The connection between the oceans and streamflow anomalies is found to be more robust during the winter (DJF). On monthly timescales, the relationship between ocean SST and streamflow is also found to be nonlinear: while high streamflow is generally related to positive Pacific and negative north Atlantic SST anomalies, low streamflow is apparently less dependent on the sign of the SST anomaly. Furthermore, a lot of the variance is still unexplained by the Pacific and Atlantic SST teleconnections.

2. Consistent with this general relationship, the highest extreme monthly flows (defined as the top 10 monthly flows throughout the record) tend to be associated with a warm equatorial Pacific and cold north Atlantic during the preceding winter (DJF). The winter precipitation patterns have wet anomalies over the southwest and southeast, and dry anomalies in the Pacific north west, consistent with the well documented ENSO teleconnection [*Ropelewski and Halpert*, 1986, ,]. The atmospheric circulation anomalies favoring extreme monthly streamflow have regions of anomalous moisture convergence at the equator and over the United States southwest. Cyclonic circulation occurs off the southwest coast of the United States, and directs southerly flow into the upper Rio Grande region. The circulation anomalies are also more robust during the winter. We conclude

that monthly streamflow is influenced by both the Pacific and Atlantic oceans, with warm equatorial Pacific and cold north Atlantic SST favoring above-normal streamflow.

3. On seasonal timescales, we find that El Niño events alter the shape of the water year hydrograph, increasing the magnitude of the peak streamflow above its longterm daily mean. This confirms the relationship noted in other studies [*Lee et al.*, 2004]. El Niño events also alter the duration of the peak, with peak flow occurring earlier and lasting longer. The complex shape of the hydrographs also suggests the varied response of upper Rio Grande streamflow to El Niño events.

4. The mechanisms explaining decadal flow variability are also investigated. The Del Norte and Otowi gages, which have the longest flow records, have high flow periods from 1900 - 1920 and 1979 - 1994, and low flow periods from 1945 - 1975, and, in the most recent decades, 1994 - 2014. The same variability is observed in precipitation records. The decadal flow variability is mediated by both the PDO and AMO. The SST composite for dry decades (1945 - 1975) minus 20th century climatology, shows SST patterns characteristic of the cool PDO and warm AMO phases (Figure 15). The wet decades demonstrate a weaker warm signal in the equatorial Pacific, consistent with other work [*Cook et al.*, 2011]. The drop in upper Rio Grande streamflow in the most recent decades (1979 - 2014) is associated with a turn to a cool PDO and warm AMO (Figure 17). For these PDO and AMO phases, there was anomalous anticyclonic flow over the north Pacific, with northeasterly flow over the upper Rio Grande. We conclude that on decadal timescales, sustained periods of both high and low flow can be explained by oceanic SST patterns.

5. Seasonal and geographical variations also impact the strength of these teleconnections. Spring to summer streamflow is most influenced by precipitation in the preceding winter-spring throughout the upper Rio Grande with all months being about equally important (Figure 5). The magnitude of the correlation between streamflow and SST in both the Pacific and Atlantic oceans is higher during the winter (DJF) than spring (MAM) (Figure 7). DJF SST therefore offers limited predictability on the sign of the upper Rio Grande streamflow anomaly; particularly for high flows. The teleconnection strength also varies within the basin. Streamflow further north in the basin (Del Norte and Chama) are less strongly correlated with the equatorial Pacific. This is consistent with the ENSO influence on southwest climate being focused to the south of the upper Rio Grande Basin.

The ocean-atmosphere configurations described explain monthly streamflow variability in the upper Rio Grande on timescales of months to decades. The ENSO, AMO and PDO teleconnections and atmospheric anomalies, are more robust during the winter, and offer limited predictability for the magnitude of streamflow. However, a lot of the variance is still unexplained by the Pacific and Atlantic SST teleconnections, suggesting the need for more work on the complex interaction of precipitation, evapotranspiration, temperature and runoff. It is hoped this study will help provide information on the drivers of upper Rio Grande streamflow, which is essential for its management and the millions of people who rely on its waters.

Acknowledgments. This work was supported by NSF award AGS-1243204 and NOAA award NA10OAR4310137 "Linking near-term future changes in weather and hy-

droclimate in western North America to adaptation for ecosystem and water management". LDEO contribution number XXXX. The streamflow data used are listed in the references, figures and available at United States Geological Survey repository online http://www.usgs.gov/water/. The precipitation data used are listed in the references, figures and available at the PRISM repository online http://www.prism.oregonstate.edu. The ERSSTV4 SST data used are listed in the references, figures and available online at http://iridl.ldeo.columbia.edu/SOURCES/.NOAA/.NCDC/.ERSST/.version4/. The ERAInterim Reanalysis data used are listed in the references, figures and available online at http://kage.ldeo.columbia.edu:81/home/.OTHER/.MoistureBudgets/.ERAInterim/.

References

Adams, D. K., and A. C. Comrie (1997), The North American Monsoon, *Bulletin of the American Meteorological Society*, *78*(10), 2197–2213, doi:10.1175/1520-0477(1997)078¡2197:TNAM¿2.0.CO;2.

Barlow, M., S. Nigam, and E. Berbery (1998), Evolution of the North American Monsoon System, *Journal of Climate*, *11*(9), 2238–2257, doi:10.1175/1520-0442(1998)011¡2238:EOTNAM¿2.0.CO;2.

Barlow, M., S. Nigam, and E. H. Berbery (2001), ENSO, Pacific decadal variability, and U.S. summertime precipitation, drought, and stream flow, *Journal of Climate*, *14*(9), 2105–2128, doi:10.1175/1520-0442(2001)014¡2105:EPDVAU¿2.0.CO;2.

Cai, W., A. Santoso, G. Wang, S.-W. Yeh, S.-I. An, K. M. Cobb, M. Collins, E. Guilyardi, F.-F. Jin, J.-S. Kug, M. Lengaigne, M. J. McPhaden, K. Takahashi, A. Timmermann, G. Vecchi, M. Watanabe, and L. Wu (2015), ENSO and greenhouse warming, *Nature Climate Change*, *5*(9), 849–859.

Cayan, D., K. Redmond, and L. Riddle (1999), ENSO and hydrologic extremes in the western United States (vol 12, pg 2881, 1999), *Journal of Climate*, *12*(12), 3516–3516.

Cook, B. I., and R. Seager (2013), The response of the North American Monsoon to increased greenhouse gas forcing, *Journal of Geophysical Research. Atmospheres*, *118*(4), 1690–1699, doi:10.1002/jgrd.50111.

Cook, B. I., R. Seager, and R. L. Miller (2011), On the causes and dynamics of the early twentieth-century North American pluvial*, *Journal of Climate*, *24*(19), 5043–5060, doi:10.1175/2011JCLI4201.1.

Daly, C., M. Halbleib, J. I. Smith, W. P. Gibson, and M. K. Doggett (2008), Physiographically sensitive mapping of climatological temperature and precipitation across the conterminous united states, *International Journal of Climatology*, *28*(15), 2031–2064, doi:10.1002/joc.1688.

Dee, D. P., S. M. Uppala, A. J. Simmons, P. Berrisford, P. Poli, S. Kobayashi, U. Andrae, M. A. Balmaseda, G. Balsamo, P. Bauer, P. Bechtold, A. C. M. Beljaars, L. van de Berg, J. Bidlot, N. Bormann, C. Delsol, R. Dragani, M. Fuentes, A. J. Geer, L. Haimberger, S. B. Healy, H. Hersbach, E. V. Hólm, L. Isaksen, P. Kållberg, M. Köhler, M. Matricardi, A. P. McNally, B. M. Monge-Sanz, J.-J. Morcrette, B.-K. Park, C. Peubey, P. de Rosnay, C. Tavolato, J.-N. Thépaut, and F. Vitart (2011), The ERA-Interim reanalysis: configuration and performance of the data assimilation system, *Quarterly Journal of the Royal Meteorological Society*, *137*(656), 553–597, doi:10.1002/qj.828.

Enfield, D. B., A. Mestas-Nunez, and P. Trimble (2001), The Atlantic Multidecadal Oscillation and its relation to rainfall and river flows in the continental U.S., *Geophysical Research Lettersesearch letters*, *28*(10), 2077–2080.

Fritze, H., I. T. Stewart, and E. Pebesma (2011), Shifts in western North American snowmelt runoff regimes for the recent warm decades, *Journal of Hydrometeorology*, *12*(5), 989–1006.

Gutzler, D. S. (2013), Streamflow projections for the Upper Gila River, *New Mexico Interstate Stream Commission*.

Hurd, B. H., and J. Coonrod (2008), *Climate change and its implications for New Mexico's water resources and economic opportunities*, New Mexico State University, Agricultural Experiment Station, Cooperative Extension Service, College of Agriculture and Home Economics.

Kahya, E., and J. A. Dracup (1993), US streamflow patterns in relation to the El Niño/Southern Oscillation, *Water Resources Research*, *29*(8), 2491–2503.

Kahya, E., and J. A. Dracup (1994), The influences of type 1 El Nino and La Nina events on streamflows in the Pacific southwest of the United States, *Journal of Climate*, *7*(6), 965–976.

Kalnay, E., M. Kanamitsu, R. Kistler, W. Collins, and D. Deaven (1996), The NCEP/NCAR 40-Year Reanalysis Project, *Bulletin of the American Meteorological Society*, *77*(3), 437–471, doi:10.1175/1520-0477(1996)077¡0437:TNYRP¿2.0.CO;2.

Khedun, C., A. Mishra, M. Özger, H. Kato-Beaudoing, J. Bolten, J. Giardino, and V. Singh (2010), *Assessing the Impacts of Climate Variability on the Water Resources in the Rio Grande/Río Bravo Basin*, pp. 69–80, American Society of Civil Engineers, doi:doi:10.1061/41114(371)9.

Larkin, N. K., and D. Harrison (2005), On the definition of El Niño and associated seasonal average US weather anomalies, *Geophysical Research Letters*, *32*(13).

Lee, S., A. Klein, and T. Over (2004), Effects of the El Niño-Southern Oscillation on temperature, precipitation, snow water equivalent and resulting streamflow in the Upper Rio Grande river basin, *Hydrological Processes*, *18*(6), 1053–1071, doi:10.1002/hyp.5511.

Llewellyn, D., and S. Vaddey (2013), *West-wide climate risk assessment: Upper Rio Grande Impact Assessment: Report*, US Department of the Interior, Bureau of Reclamation, Upper Colorado Region, Albuquerque Area Office.

McCabe, G., M. Palecki, and J. Betancourt (2004), Pacific and Atlantic Ocean influences on multidecadal drought frequency in the United States, *Proceedings of the National Academy of Sciences*, *101*(12), 4136–41, doi:10.1073/pnas.0306738101.

Notaro, M., Z. Liu, R. G. Gallimore, J. W. Williams, D. S. Gutzler, and S. Collins (2010), Complex seasonal cycle of ecohydrology in the southwest United States, *Journal of Geophysical Research: Biogeosciences (2005–2012)*, *115*(G4).

Nowak, K., M. Hoerling, B. Rajagopalan, and E. Zagona (2012), Colorado River basin hydroclimatic variability, *Journal of Climate*, *25*(12), 4389–4403.

Pascolini-Campbell, M. A., R. Seager, D. S. Gutzler, B. I. Cook, and D. Griffin (2015), Causes of interannual to decadal variability of Gila River streamflow over the past century, *Journal of Hydrology: Regional Studies*, *3*, 494–508, doi: http://dx.doi.org/10.1016/j.ejrh.2015.02.013.

Ropelewski, C. F., and M. Halpert (1996), Quantifying Southern Oscillation-Precipitation Relationships, *Journal of Climate*, *9*(5), 1043–1059, doi:10.1175/1520-0442(1996)009¡1043:QSOPR¿2.0.CO;2.

Ropelewski, C. F., and M. S. Halpert (1986), North American Precipitation and Temperature Patterns Associated with the El Niño/Southern Oscilla-

tion (ENSO), *Monthly Weather Review*, *114*(12), 2352–2362, doi:10.1175/1520-0493(1986)114¡2352:NAPATP¿2.0.CO;2.

Ropelewski, C. F., and M. S. Halpert (1989), Precipitation Patterns Associated with the High Index Phase of the Southern Oscillation, *Journal of Climate*, *2*(3), 268–284, doi:10.1175/1520-0442(1989)002¡0268:PPAWTH¿2.0.CO;2.

Ruff, T. W., Y. Kushnir, and R. Seager (2011), Comparing Twentieth and Twenty-First-Century patterns of Interannual Precipitation Variability over the Western United States and Northern Mexico, *Journal of Hydrometeorology*, *13*(1), 366–378, doi:10.1175/JHM-D-10-05003.1.

Schubert, S. (2009), A U.S. CLIVAR Project to Assess and Compare the Responses of Global Climate Models to Drought-Related SST Forcing Patterns: Overview and Results, *Journal of climate*, *22*(19), 5251–5272, doi:10.1175/2009JCLI3060.1.

Seth, A., S. A. Rauscher, M. Biasutti, A. Giannini, and S. J. Camargo (2013), CMIP5 projected changes in the annual cycle of precipitation in monsoon regions, *Journal of Climate*, *26*(19), 7328–7351, doi:10.1175/JCLI-D-12-00726.1.

Smith, T. M., R. W. Reynolds, T. C. Peterson, and J. Lawrimore (2008), Improvements to NOAA's Historical Merged Land–Ocean Surface Temperature Analysis (1880–2006), *Journal of Climate*, *21*(10), 2283–2296, doi:10.1175/2007JCLI2100.1.

Stewart, I. T., D. Cayan, and M. D. Dettinger (2005), Changes toward earlier streamflow timing across western North America, *Journal of climate*, *18*(8), 1136–1155.

Thomas, B. E. (2007), Climatic fluctuations and forecasting of streamflow in the lower Colorado River basin, *Journal of the American Water Resources Association*, *43*(6), 1550–1569.

Ting, M., Y. Kushnir, and C. Li (2014), North Atlantic Multidecadal SST Oscillation: External forcing versus internal variability, *Journal of Marine Systems*, *133*, 27–38, doi:http://dx.doi.org/10.1016/j.jmarsys.2013.07.006.

Trenberth, K. E., G. W. Branstator, D. Karoly, A. Kumar, N.-C. Lau, and C. Ropelewski (1998), Progress during TOGA in understanding and modeling global teleconnections associated with tropical sea surface temperatures, *Journal of Geophysical Research: Oceans*, *103*(C7), 14,291–14,324, doi:10.1029/97JC01444.

Woodhouse, C., D. Meko, D. Griffin, and C. Castro (2013), Tree rings and multiseason drought variability in the lower Rio Grande Basin, *Water Resources Research*, *49*(2), 844–850.

Woodhouse, C. A., D. W. Stahle, and J. Villanueva Diaz (2012), Rio Grande and Rio Conchos water supply variability over the past 500 years, *Climate Research*, *51*(2), 147.

Zhang, Y., J. M. Wallace, and D. S. Battisti (1997), ENSO-like Interdecadal Variability: 1900–93, *Journal of Climate*, *10*(5), 1004–1020, doi:10.1175/1520-0442(1997)010¡1004:ELIV¿2.0.CO;2.

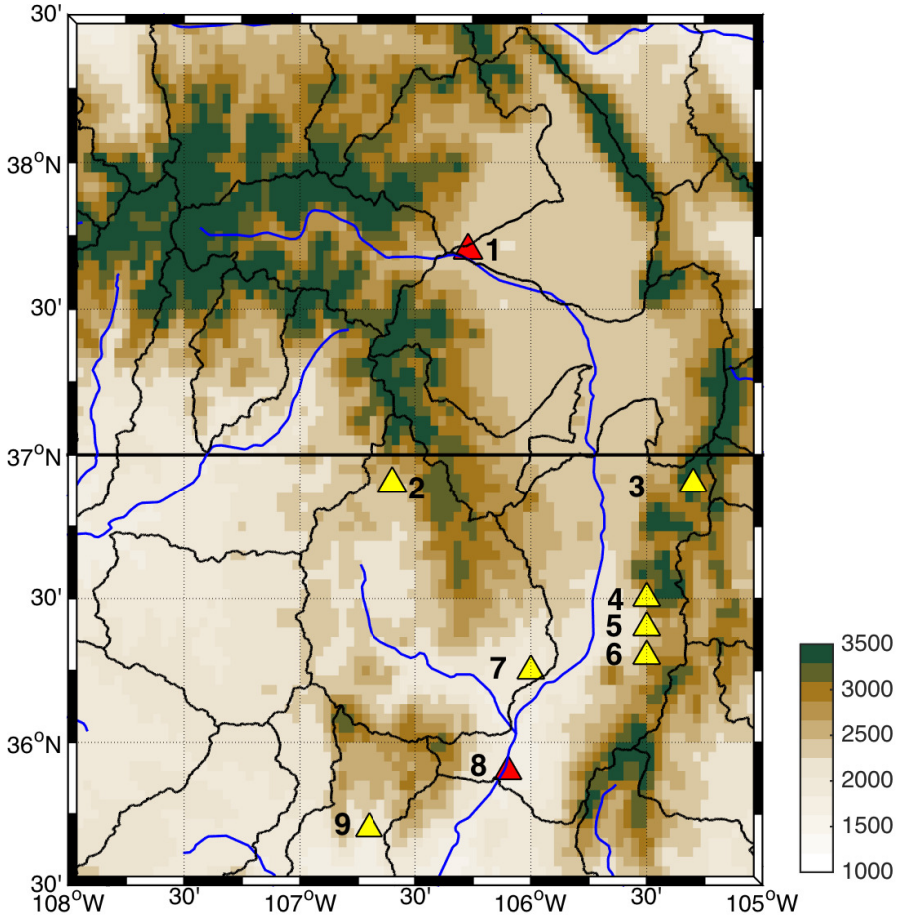

Figure 1. Map showing elevation (meters), 8-digit hydrologic units, and location of USGS stream gages used in this study: 1) Del Norte, 2) Rio Chama, 3) Santistaven creek, 4) Rio Hondo, 5) Rio Lucero, 6) Rio Pueblo de Taos near Taos, 7) Rio Ojo, 8) Otowi, 9) Jemez river. Red marker indicates stream gage is located on main stem, yellow marker indicates stream gage is located on a tributary.

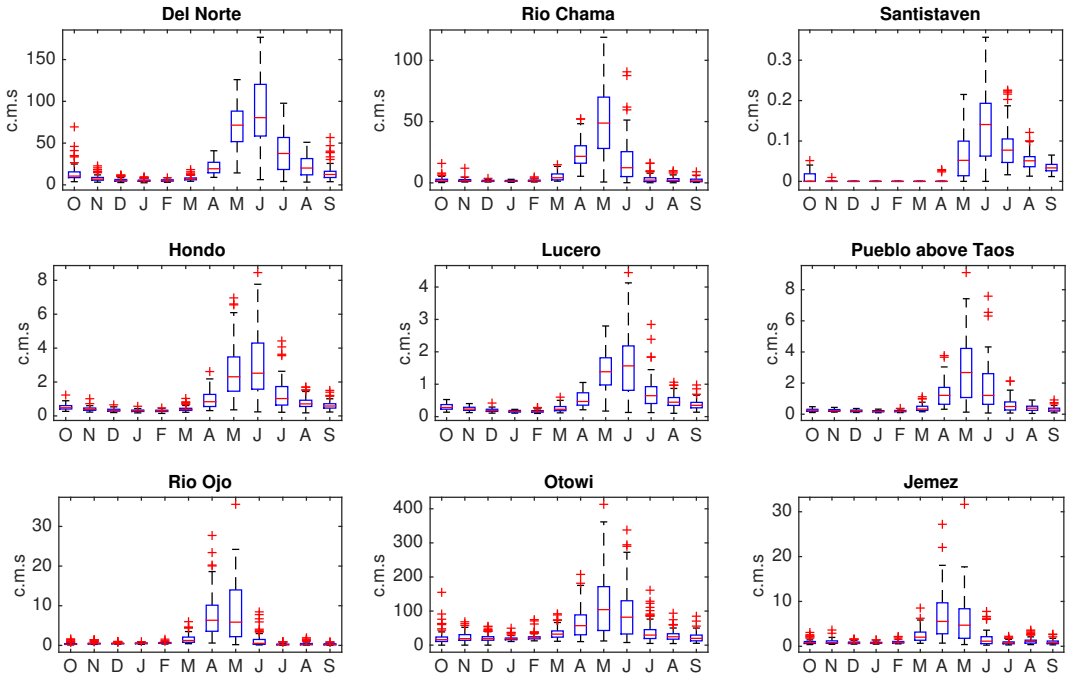

Figure 2. Boxplots of monthly streamflow (c.m.s.) over length of record for each stream gage. For each boxplot, the central mark is the median, the edges of the box are the 25th and 75th percentiles, the whiskers extend to the most extreme data points not considered outliers, and outliers are plotted individually.

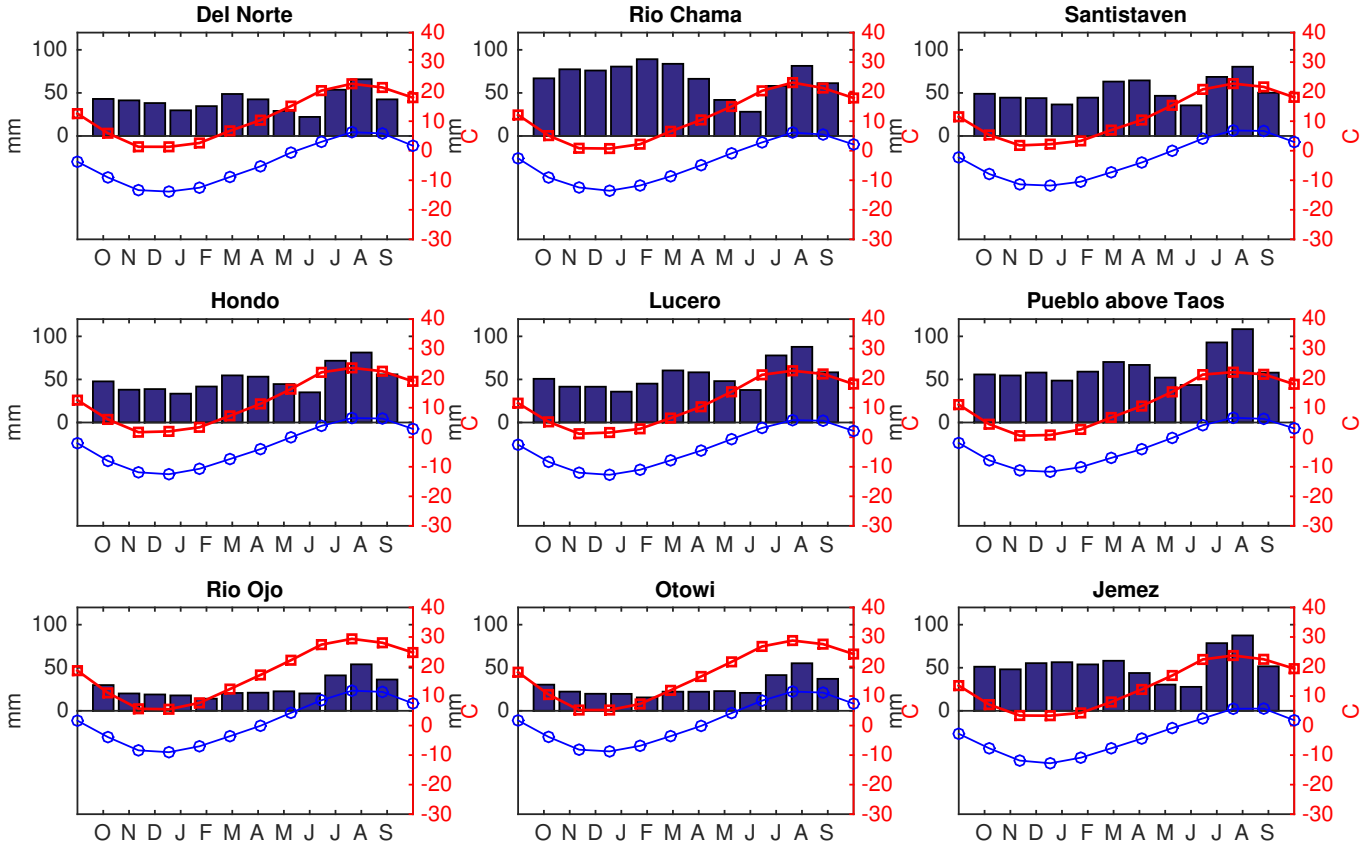

Figure 3. Seasonal cycle of PRISM precipitation (bars), minimum temperature (blue line) and maximum temperature (red line) for records of each stream gage.

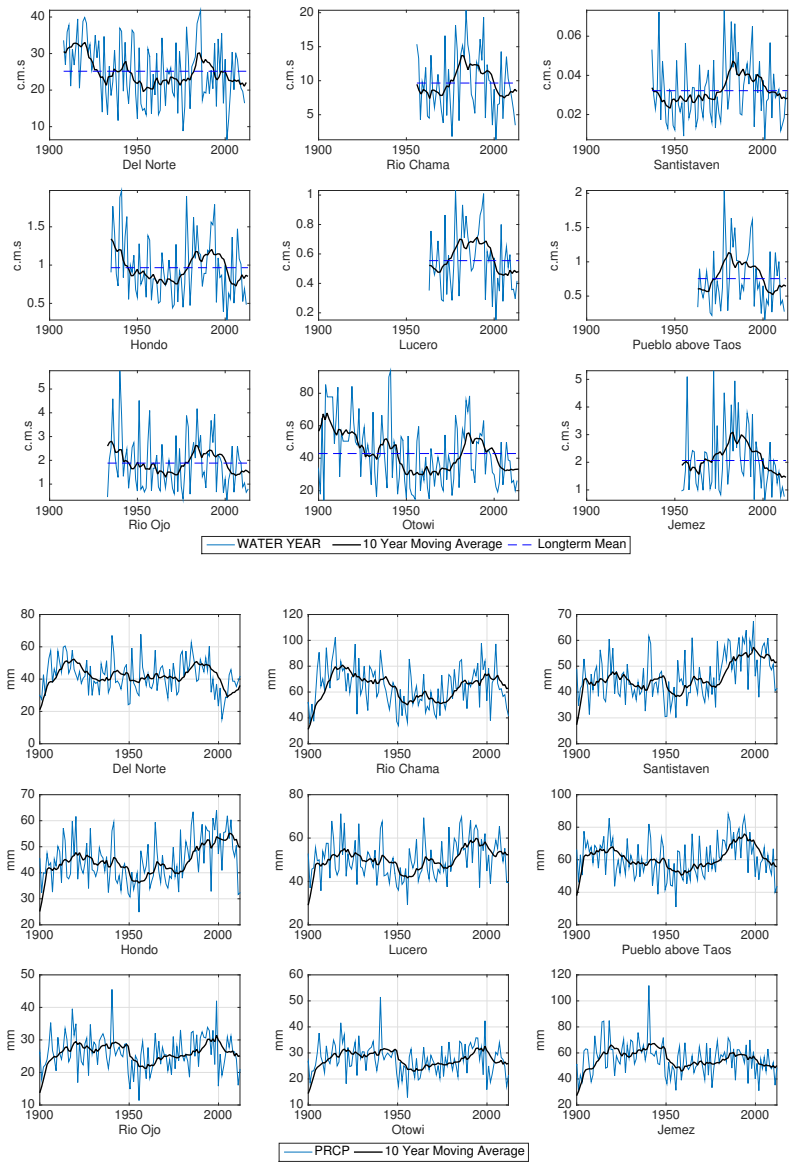

Figure 4. Top: Timeseries for mean water year (October to September) streamflow (c.m.s.) for each stream. Blue line is water year mean, black line is 10 year moving average and black-dashed line is long term mean for each flow. Bottom: Timeseries for annually averaged water year (October to September) (blue line) and 10 year moving average (black line) PRISM precipitation area-averaged over the drainage basin of each stream gage.

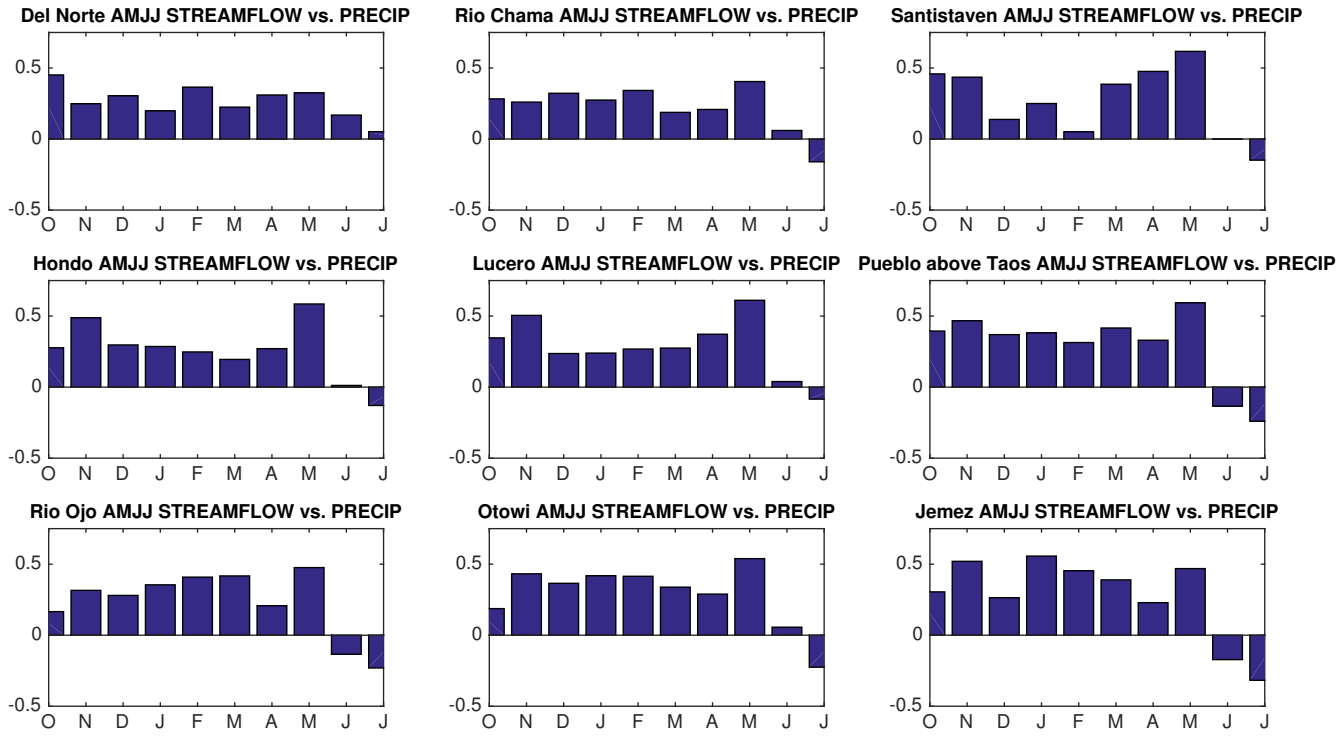

Figure 5. Cross correlation for log of spring-summer (AMJJ) streamflow with monthly PRISM precipitation area averaged over each drainage basin.

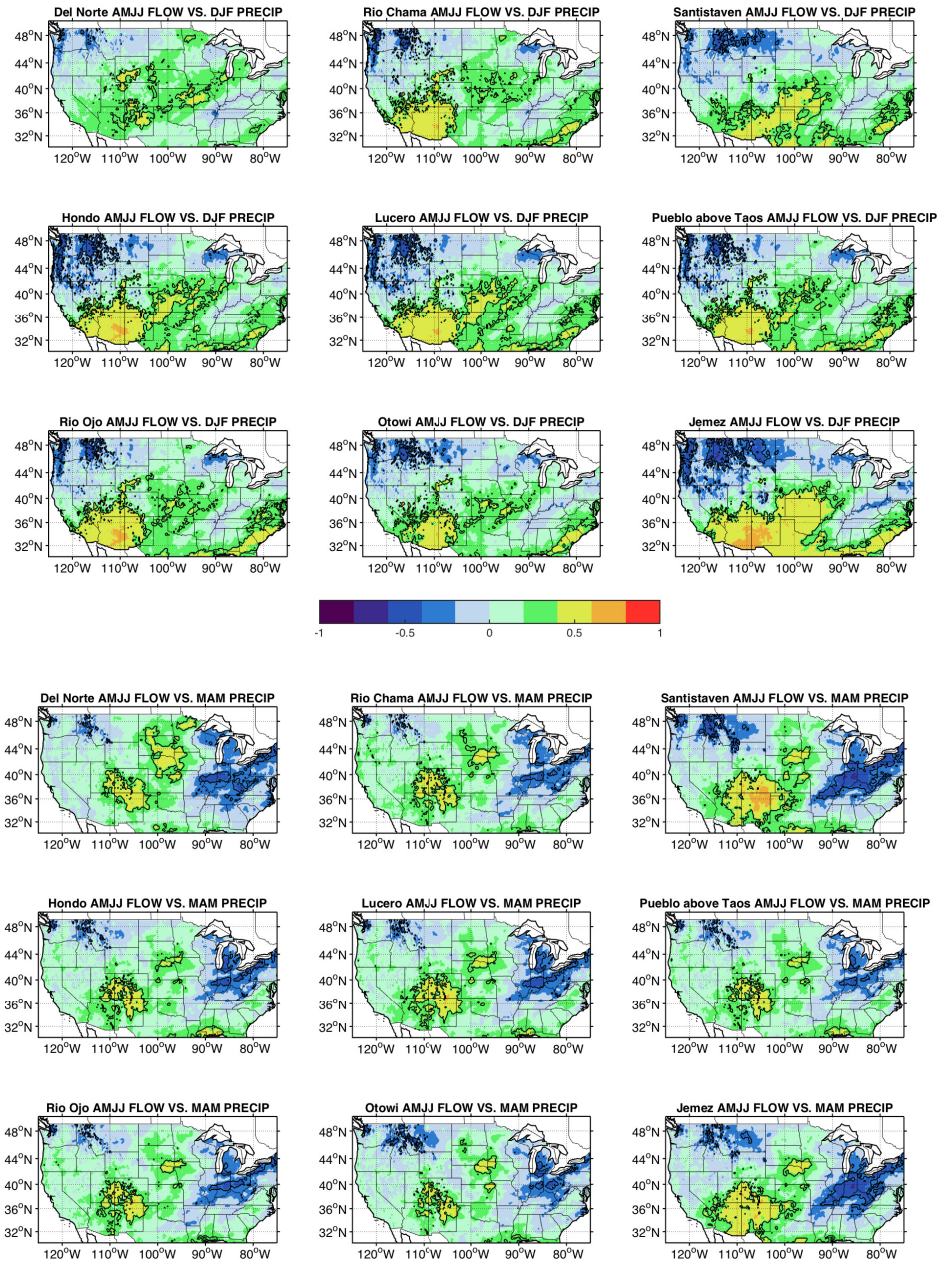

Figure 6. Correlation of AMJJ streamflow with PRISM precipitation during preceding DJF (top panels) and MAM (bottom panels) seasons. Colorbar indicates magnitude of the correlation. Areas that are significant at $p<0.05$ lie within the black contour.

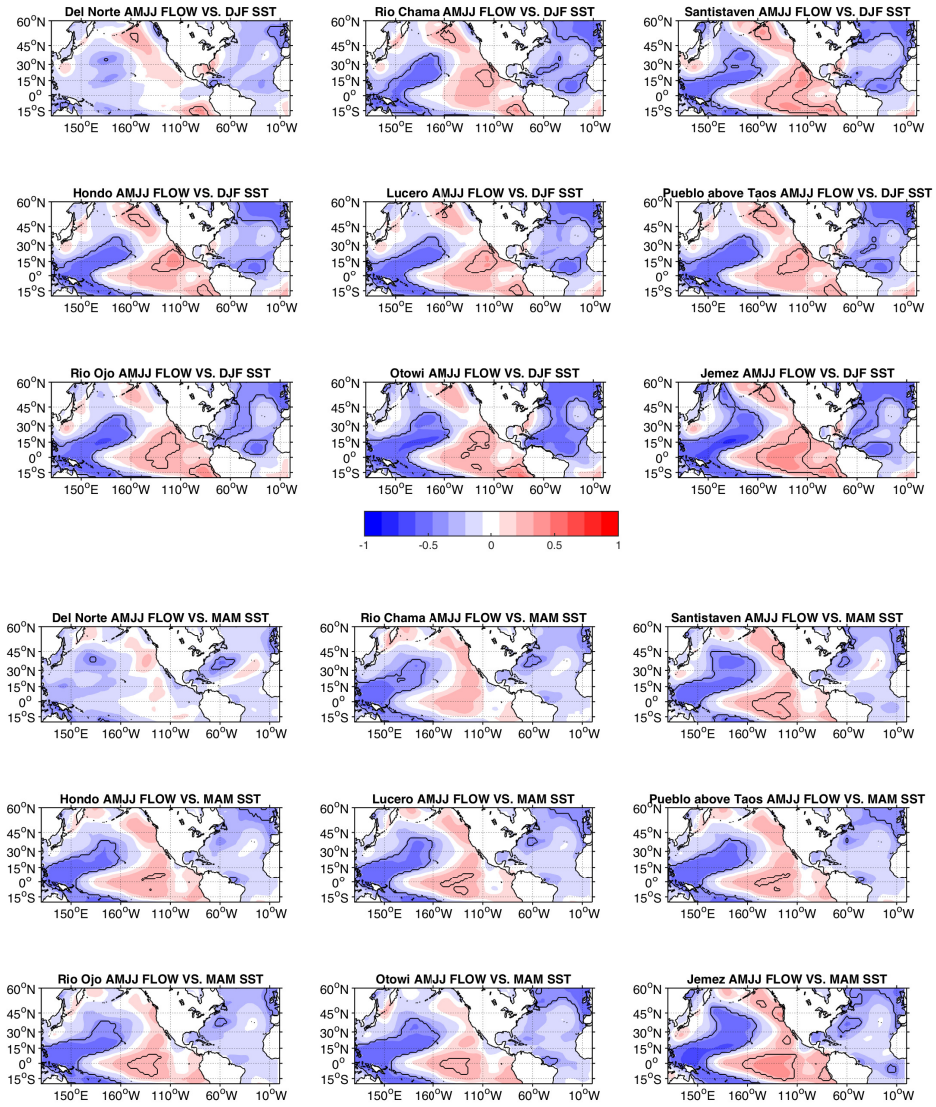

Figure 7. AMJJ streamflow correlated with ERSST V4 SST for preceding DJF (top panels) and MAM (bottom panels). Colorbar indicates magnitude of the correlation. Areas that are significant at $p<0.05$ lie within the black contour.

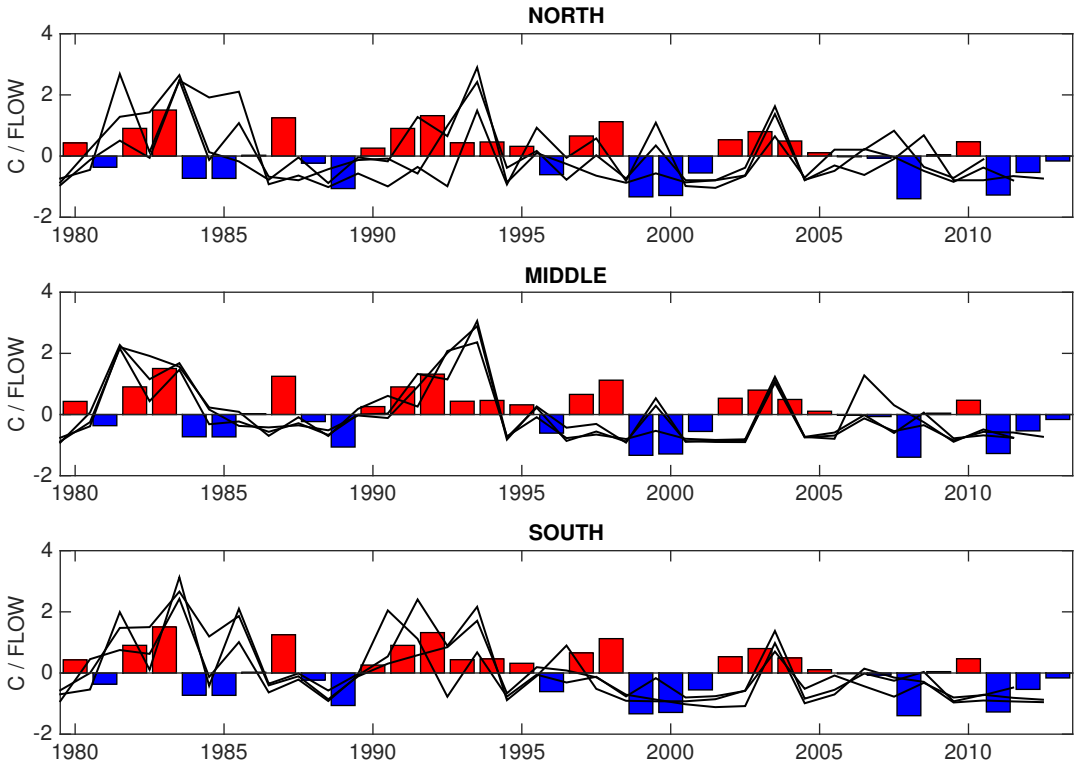

Figure 8. Bar graph shows NINO3.4 SST anomaly for the DJF season, and black lines show the standardized flow anomaly for the maximum flow occurring in each water year. These are arranged as follows: the three most northern gages (Del Norte, Rio Chama, Santistaven) (top panel), middle gages (Hondo, Lucero, Pueblo) (middle panel) and southern gages (Ojo, Otowi, Jemez) (bottom panel).

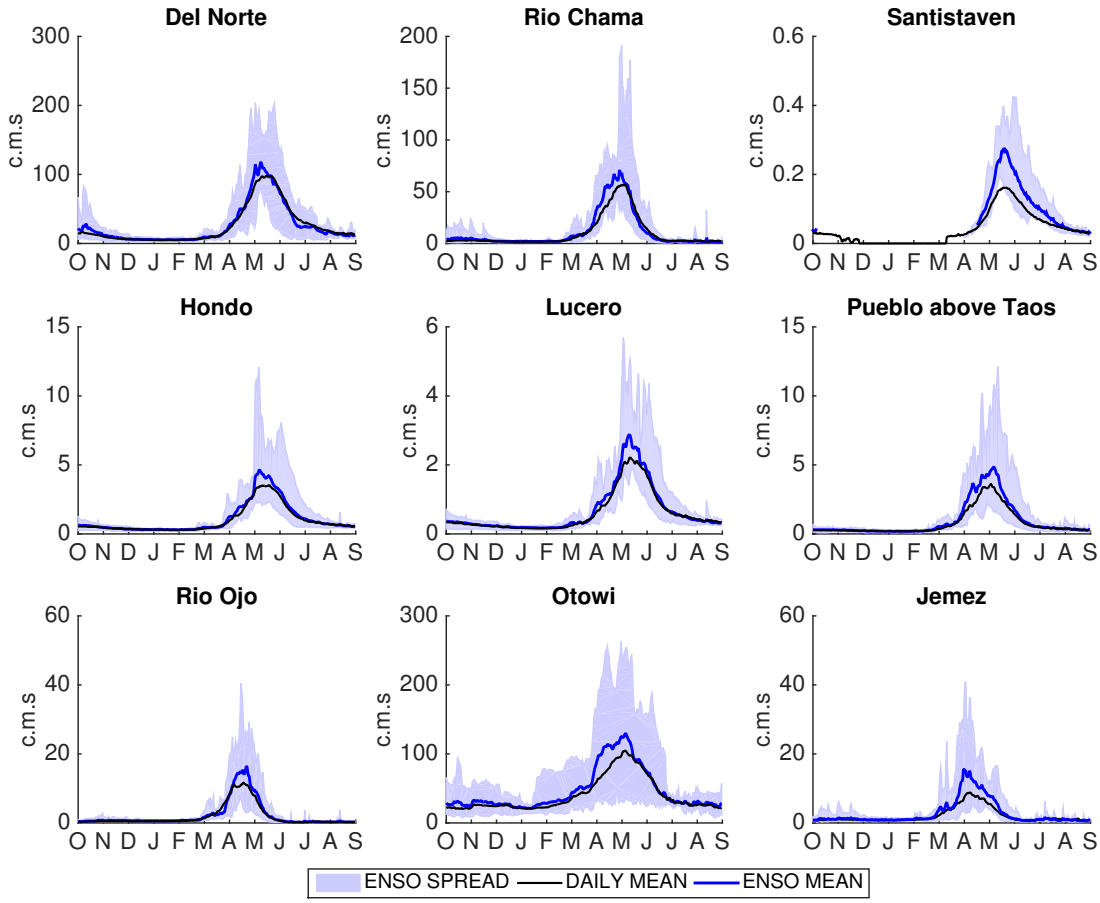

Figure 9. Spread of flow anomalies in daily data occurring during El Niño events in the 1980 to 2015 period (1982/83, 1986/87, 1991/92, 1997/98, 2002/03, 2004/05, 2006/07, 2009/10) (blue shading), mean of El Niño events (blue line), as well as the long term daily mean statistics (black line) (USGS).

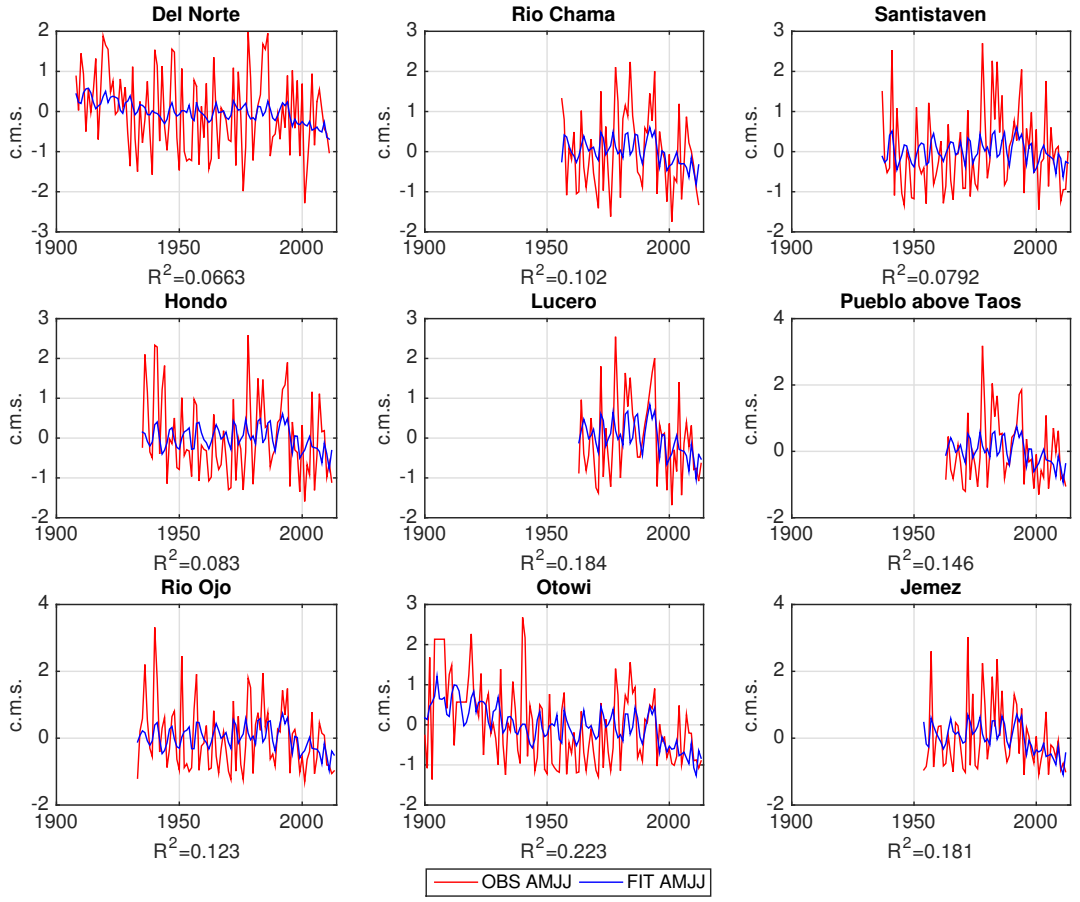

Figure 10. Results from a multiple linear regression of DJF NINO3.4 index and DJF TNA index with annual spring-summer (AMJJ) streamflow anomaly. The predicted (blue line) and observed AMJJ streamflow anomaly (red line) are plotted for each stream gage over the length of the dataset. R^2 values for the multiple regression are shown below each timeseries.

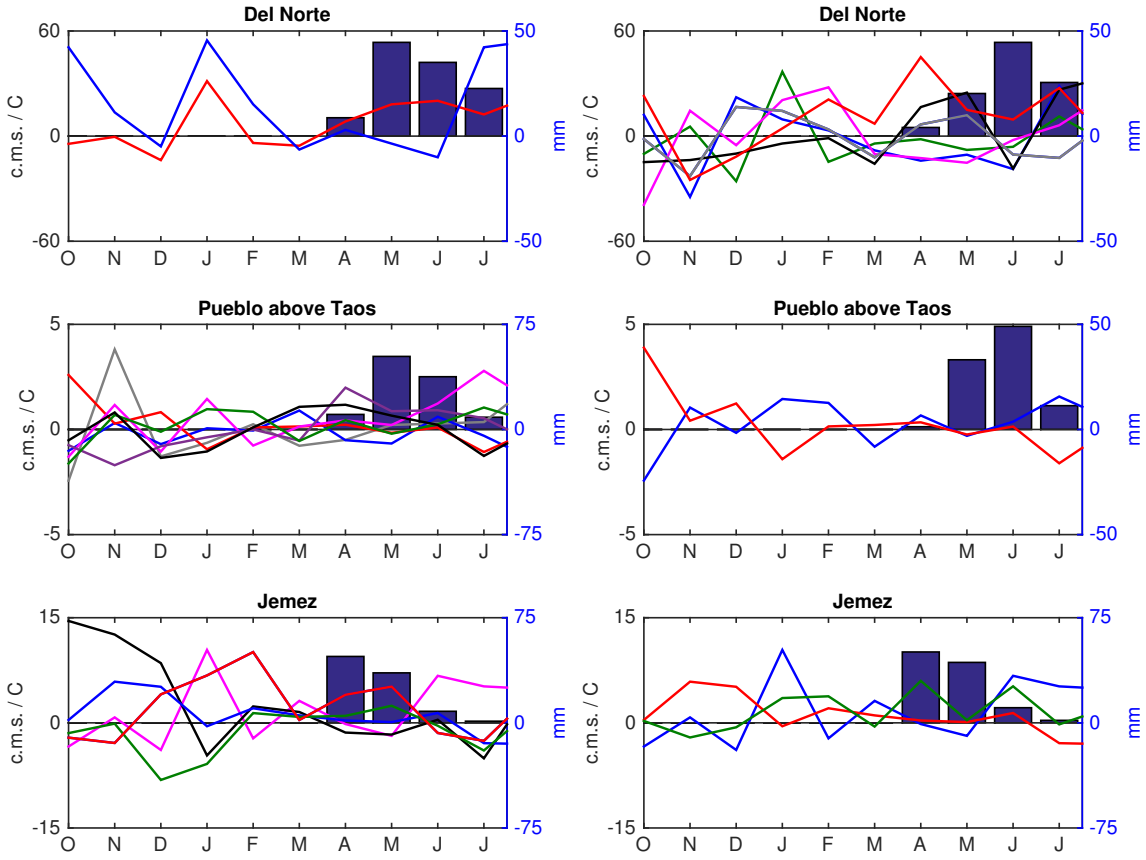

Figure 11. Top 10 monthly flow composite with the associated preceding and concurrent precipitation anomalies (October - July) (lines) as well as monthly flow anomalies (AMJJ; bars).

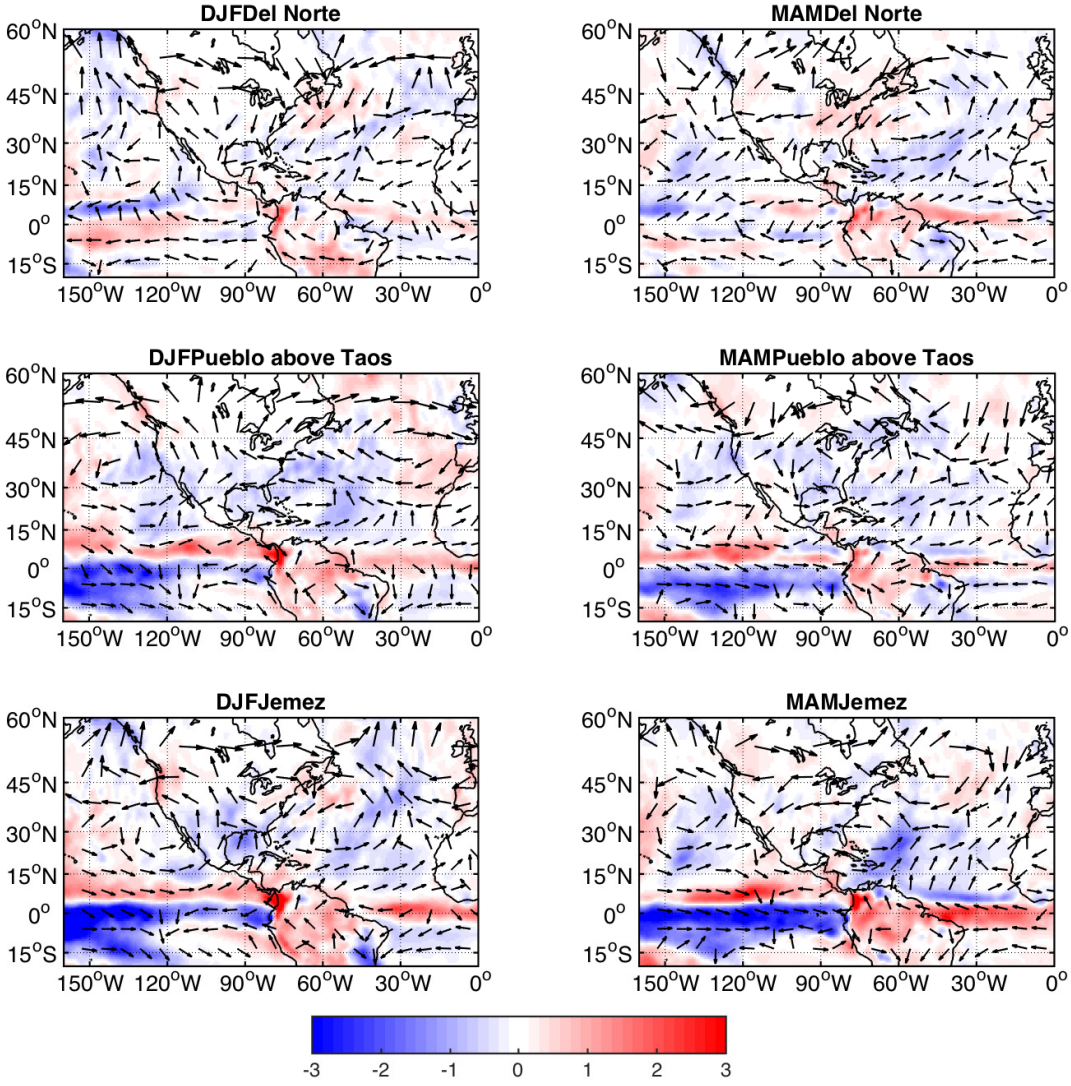

Figure 12. Top 10 monthly flow composites for ERA-Interim vertically integrated moisture transport anomaly (vectors) and its divergence (colors) in the preceding DJF (left panels) and MAM (right panels) season. Results for Del Norte (top panels), Pueblo (middle panels) and Jemez (bottom panels). Colorbar indicates the magnitude of the divergence (1.15710^{-8} x m s^{-1}).

.

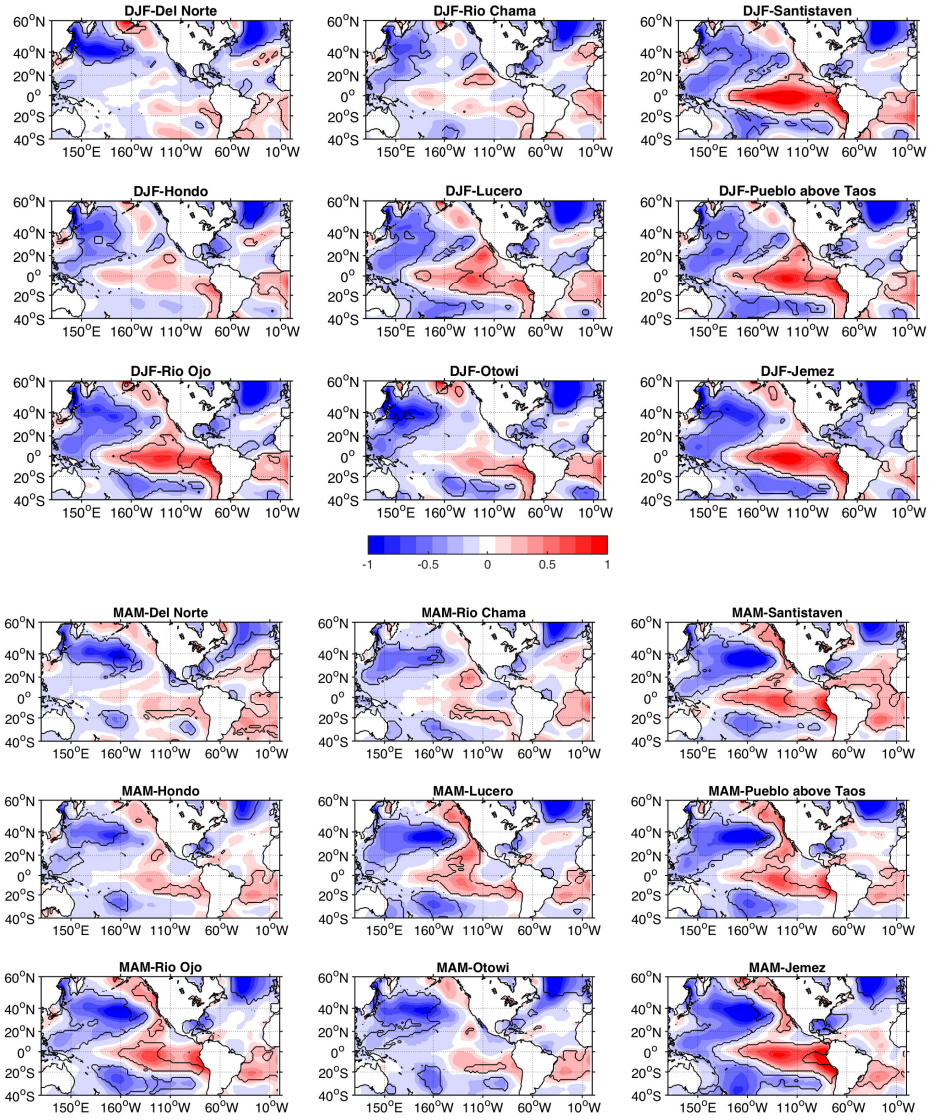

Figure 13. Composite for SST anomalies across the years containing the top 10 monthly flows from 1980 to 2014 in the preceding DJF (top panels) and MAM (bottom panels) season. Colorbar shows magnitude of SST anomaly (°C). Contour indicates regions where at least 7 of the 10 months have the same sign as the mean SST, and also where absolute anomaly in SST is greater than 0.5σ of the longterm seasonal variability.

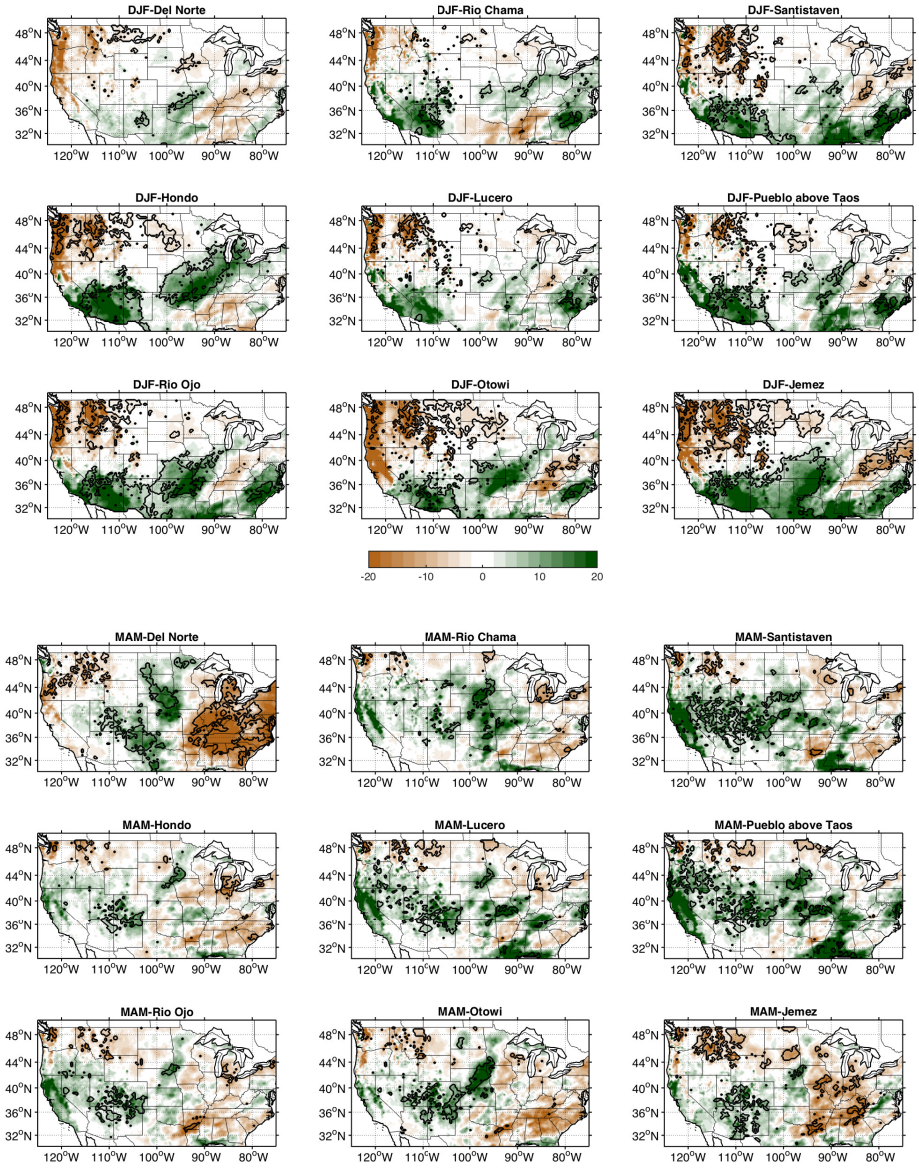

Figure 14. Composite for precipitation anomalies across the years containing the top 10 monthly flows from 1980 to 2014 in the preceding DJF (top panels) and MAM (bottom panels) season. Contour indicates regions where at least 7 of the 10 months have the same sign as the mean precipitation, and also where absolute anomaly in precipitation is greater than 0.5σ of the longterm seasonal variability.

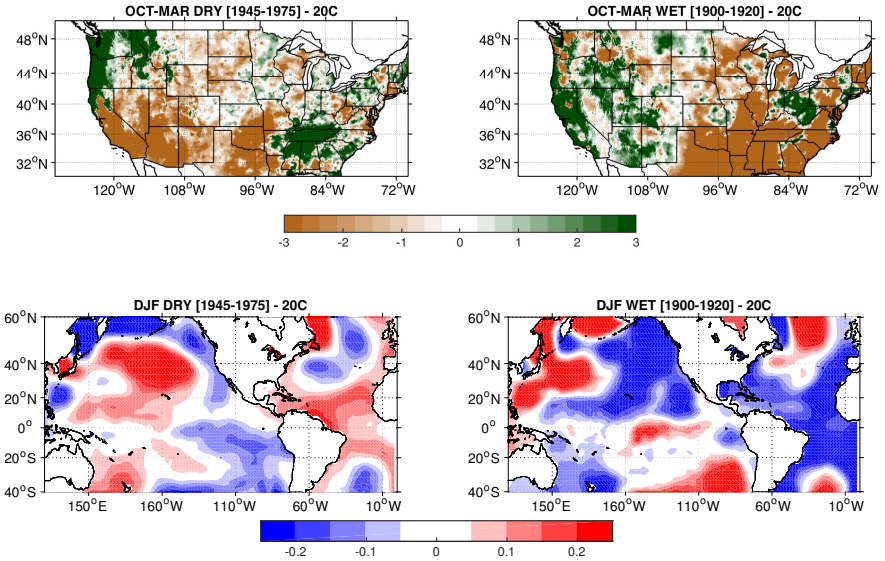

Figure 15. Dry decades (1945-1975) minus detrended 20th century climatology (left panels) and wet decades (1900-1920) minus detrended 20th century climatology (right panels) for water year composite PRISM precipitation (top) and DJF ERSST V4 SST (bottom).

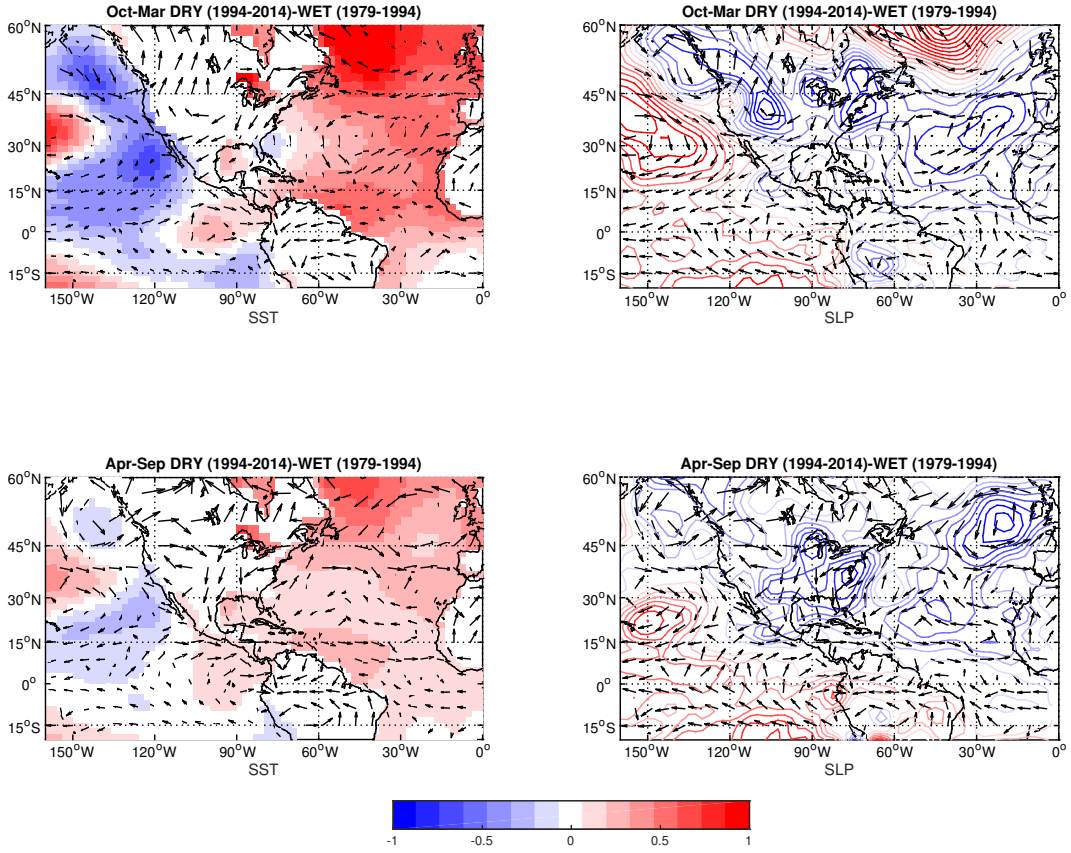

Figure 16. Top panels: Dry decades (1994-2014) minus wet decades (1979-1994) composites for ERA-Interim vertically integrated moisture transport anomaly (vectors), ERSST V4 SST (shading) (left) and NCEP/NCAR Reanalysis SLP (shading) (right) for October to March. Bottom panel: Same as above for April to September.

Table 1. Summary of USGS station data

Gage Name	Gage Number	Temporal Availability (monthly statistics)	Drainage Area (sq mi)	Elevation (feet above NGVD29)	Correlation: Del Norte (Otowi) (r-value)
Del Norte	08220000	1908 - 2015	1320	7980	1.00 (0.84)
Rio Chama	08284100	1955 - 2014	480	7083	0.84 (0.92)
Santistaven	08253500	1937 - 2014	2.15	9520	0.75 (0.79)
Hondo	08267500	1934 - 2015	36.2	7650	0.69 (0.86)
Lucero	08271000	1913 - 2014	16.6	8051	0.72 (0.84)
Pueblo	08269000	1913 - 2014	66.6	7380	0.69 (0.87)
Ojo	08289000	1932 - 2016	419	6358	0.75 (0.91)
Otowi	08313000	1895 - 2016	14300	5488	0.84 (1.00)
Jemez	08324000	1936 - 2016	470	5622	0.71 (0.81)